AIAA 95-1317
Effects of Stiffening and Mechanical Load on Thermal Buckling of Stiffened Cylindrical Shells

Theodore F. Johnson
Michael F. Card
NASA Langley Research Center
Hampton, VA 23681-0001

Presented at the AIAA/ASME/ASCE/AHS/ASC 36th Structures, Structural Dynamics and Materials Conference
April 10–12, 1995 / New Orleans, LA
Thermal Structures Category

4. Table 2 contains the boundary conditions for studies of longitudinally stiffened shells without ring frames where symmetry is employed at one end of the shell. Table 3 displays the boundary conditions for full-length ring- and stringer-stiffened shells. Table 4 contains boundary conditions used for a study of the interior behavior of the shell where symmetry is employed at both ends.

Table 1. Material properties and geometry of members of an internally stiffened shell.

Member	E ksi.	ν	α per °F	A in^2	I in^4	GJ $lbs\text{-}in^2$	e in.
Skin	$14.5x10^3$	.30	$5.0x10^{-5}$	-	-	-	-
Ring	$16.4x10^3$	-	-	.246	.1377	3477	-1.992
Stringer	$16.4x10^3$	-	-	.0495	.004083	.000	-.342

E - Modulus of Elasticity
ν - Poisson's ratio
α - Coefficient of thermal expansion
A - Area
I - Moment of inertia
GJ - Torsional Rigidity
e - Eccentricity measured from mid-plane of the shell wall to the centroid of the stiffening member (positive if located on the outer surface, Fig. 3)

Table 2. Boundary conditions for interior shell models employing symmetry.

Pre-Buckling

Left End	Right End (Plane of Symmetry)
u = free	u = fixed
v = fixed	v = free
w = fixed	w = free
$w_{,x}$ = free	$w_{,x}$ = fixed

Buckling

Left End	Right End (Plane of Symmetry)
u = free	u = fixed
v = fixed	v = free
w = fixed	w = free
$w_{,x}$ = free	$w_{,x}$ = fixed

The shell is loaded with axial line loads and a uniform temperature change, Fig. 3. The axial line loads are applied at the two ends in opposing directions on the centroid of the shell and stringer cross-section. The uniformly distributed axial line load represents an approximation to the maximum load experienced in bending by the fuselage. A uniform temperature change is applied to the skin only. The temperature change is not applied to the rings, stiffeners or bulkheads. A zero temperature change is applied to the skin where the bulkheads and rings come into contact with the skin; as a result, a temperature gradient is formed in the axial direction. The described temperature loading occurs as the vehicle climbs to altitude. As the SST ascends, the outside temperature rises and the internal stiffeners and bulkheads remain cool, not only because of the thermal mass of the members, but also because of climate conditions inside the cabin. All of the loads on the shell are applied to produce the worst case conditions, yielding conservative results.

Table 3. Boundary conditions for full-length ring- and stringer-stiffened shells.

Pre-Buckling

Left End	Center	Right End
u = free	u = fixed	u = free
v = fixed	v = free	u = free
w = fixed	w = free	w = fixed
$w_{,x}$ = free	$w_{,x}$ = free	$w_{,x}$ = free

Buckling

Left End	Center	Right End
u = free	u = fixed	u = free
v = fixed	v = free	v = fixed
w = fixed	w = free	w = fixed
$w_{,x}$ = free	$w_{,x}$ = free	$w_{,x}$ = free

The impact of length of the shell and the number of rings on thermal buckling results is the first study conducted using BOSOR4. In Fig. 4, results are presented showing the difference in the axial or thermal buckling load as the number of rings increase. When considering four or more rings, the results do not vary for either temperature loading or axial loading. There is a small change in wave number, but not a significant difference in temperature or axial buckling load.

Since the addition of rings would not result in a more accurate solution, a six-ring model is used to represent a

complete shell. The restriction of the shell to a length of six rings eliminates general instability as a mode of failure in the present studies. Thus, the buckling interaction investigated herein is between panel instability from axial compression and local buckling from circumferential stress due to end constraints and temperature change.

Table 4. Boundary conditions for single-ring models employing symmetry at both ends.

Pre-Buckling

Left End	Right End
u = free	u = fixed
v = fixed	v = free
w = free	w = free
$w,_x$ = fixed	$w,_x$ = fixed

Buckling

Left End	Right End
u = free	u = fixed
v = fixed	v = free
w = free	w = free
$w,_x$ = fixed	$w,_x$ = fixed

III. Results and Discussion

It was suspected that two distinct buckling modes would have a direct impact on the shape of the interaction curve. Hoff[5] showed that when a shell buckles because of thermal loads, local instability at the boundaries was usually the mode of failure. Local instability can occur when the boundaries were rigid compared to the shell and caused high circumferential stress. Panel instability was usually associated with axial loading or end shortening, Anderson.[6]

In the present study of shell buckling behavior, it is found that eccentricity of the longitudinal stiffening has a large effect. Eccentricity is measured from the centroid of the stiffening member to the reference surface of the shell, Fig. 3. To highlight this effect, results for shells without rings are presented first.

Longitudinally Stiffened Shells

Results for the buckling interaction curve for longitudinally stiffened shells are presented in Figs. 5 and 6. The buckling interaction curve and mode shapes are for the geometry given in Fig. 2, but without ring frames. The longitudinal stiffeners are located either on the internal or external surface of the shell. The results in Figs. 5 and 6 suggest that the interaction between buckling modes (panel vs. local) are quite separate with no transitions between modes.

The shell buckles because of panel instability in the portion of the buckling interaction curve with circular symbols in Figs. 5 and 6. Panel instability is due to axial load. The mode shape for this type of failure is indicated on the figures. The location of failure in the shell is depicted by the maximum peaks on the graphs. The shell buckles because of local instability in the portion of the curve with square symbols in Figs. 5 and 6. Local instability is due to high circumferential stresses caused by the imposed temperature change and end constraints. The associated mode shape is indicated on the figures.

The internally stiffened shell under only temperature loading, Fig. 5, can tolerate a temperature change of almost three times the temperature change withstood by the externally stiffened shell, Fig. 6 ($T_{int.}$ = 1003°F vs. $T_{ext.}$ = 340° F). This extreme difference is a very interesting phenomena for thermally loaded shell structures. The externally stiffened shell can withstand almost twice the axial load carried by the internally stiffened shell ($Nx_{int.}$ = 561 lbs/in. vs. $Nx_{ext.}$ = 922 lbs/in.) for axial loading only. The latter result is well known for longitudinally stiffened shells when comparing the relative strength of external stiffening to internal stiffening.

Ring- and Stringer-Stiffened Shells

The buckling interaction curve for a ring- and stringer-stiffened shell with internal longitudinal stringers at an eccentricity of -0.342 inches is presented in Fig. 7. The buckling interaction curve has a distorted but similar shape compared to that produced by Chang and Card.[4] In the buckling interaction curve presented in Fig. 7, two distinct buckling modes are present and both influence the shape of the curve. The shell fails from axial load, i.e., panel instability, in the portion of the curve with circular symbols. The associated mode shape is indicated in Fig. 7. Buckling under axial loading is caused by high stresses in the axial direction of the shell. In the portion of the curve with square symbols, failure is caused by temperature change or local instability (see Fig. 7). Buckling under temperature load is induced by high circumferential stresses developed in the skin at the cool bulkheads (edge effect). The center portion of the curve (portion with triangular symbols) exhibits where the two mode shapes interact with each other forming a hybrid or combined mode shape. Failure of the shell is caused by combined panel and local instability, Fig. 7.

During the generation of the buckling interaction curve in Fig. 7 with axial load as the eigenvalue parameter, it was found that multiple solutions could exist beyond the portion of the curve dominated by axial load (portion of curve with circular symbols). Temperature was used as the eigenvalue parameter to overcome this difficulty.

In Table 5, it can be seen that the wave numbers decrease as the axial load changes from tension to compression (compression is positive). This trend shows that the mode shapes mutate along the curve, Fig. 7, in a continual fashion. The mode shape quickly changes from panel instability to the hybrid mode shape at the distortion in the curve as the curve is traversed from above. However, there is a smooth transition from local instability to the hybrid mode shape as the buckling interaction curve is traversed from below.

As the centroid of the longitudinal stiffeners is moved through the thickness of the shell, the buckling interaction curve distorts even more. The results in Fig. 8 are for the shell with the centroid of the stringers at the shell's reference surface or mid-plane (eccentricity = 0.000 inches). The longitudinal stiffeners in Fig. 9 are external to the shell, at an eccentricity of 0.342 inches. The buckling modes remain the same in Figs. 7, 8 and 9, but their shape varies with eccentricity. When the eccentricity of the stringers is varied, the shape of the buckling interaction curve develops a large distortion. This distortion occurs where hybrid buckling modes are located. The distortion is most pronounced when the longitudinal stiffeners are fully external to the shell. All of the results characterized in the two previous paragraphs for the internally stiffened shell (eccentricity = -0.342 inches) remain the same, but the shape of the buckling interaction curve changes significantly, Fig. 8 and Fig. 9.

In Fig. 10, the buckling interaction curves for the three discussed eccentricities are superimposed on one graph. In this figure the dramatic effect of changing the eccentricities can be seen. As the centroid of the stringers is moved through the mid-plane of the shell wall (internal to external), the maximum axial load decreases then increases, but the maximum temperature load continually decreases. The axial load increases by a factor of 1.4 ($Nx_{int.}$ = 4122 lbs/in. vs. $Nx_{ext.}$ = 5568 lbs/in.) for longitudinal stiffening with no temperature change. The maximum temperature change decreases by a factor of over 2.0 between internal and external stiffening ($T_{int.}$ = 626°F vs. $T_{ext.}$ = 300°F when there is no axial load).

The three-dimensional plot, Fig. 11, shows a surface envelope of buckling results that displays how the distortion of the buckling interaction curve changes as the eccentricity is varied The reduction in buckling temperature and increase in axial load can also be seen in Fig. 11. The solution surface shows that as the centroid of the stringers is moved closer to the reference surface, not only does the ability of the shell to resist temperature load decrease, so does its ability to withstand axial load.

Table 5. Buckling Results from BOSOR4 for an internally stiffened shell with ring frames.

Critical Pressure Psig.	Critical Temp. ° F.	Critical Nx Lbs/In.	Circum-ferential Wave Number	Eccen-tricity* In.
0.	623.5	-600.0	67	-0.3420
0.	623.9	-400.0	66	-0.3420
0.	624.5	-200.0	65	-0.3420
0.	626.5	000.0	63	-0.3420
0.	624.2	200.0	62	-0.3420
0.	619.2	400.0	60	-0.3420
0.	610.3	600.0	59	-0.3420
0.	598.3	800.0	58	-0.3420
0.	583.9	1000.0	57	-0.3420
0.	566.6	1200.0	56	-0.3420
0.	549.3	1400.0	55	-0.3420
0.	530.8	1600.0	54	-0.3420
0.	511.4	1800.0	53	-0.3420
0.	490.8	2000.0	52	-0.3420
0.	469.1	2200.0	51	-0.3420
0.	446.0	2400.0	49	-0.3420
0.	421.3	2600.0	47	-0.3420
0.	399.9	2765.0	46	-0.3420
0.	375.0	2942.0	44	-0.3420
0.	350.1	3102.0	42	-0.3420
0.	324.9	3249.0	39	-0.3420
0.	300.0	3376.0	37	-0.3420
0.	275.0	3486.0	34	-0.3420
0.	250.0	3580.0	32	-0.3420
0.	225.0	3664.0	30	-0.3420
0.	200.0	3734.0	28	-0.3420
0.	175.0	3797.0	27	-0.3420
0.	150.0	3853.0	26	-0.3420
0.	125.0	3905.0	25	-0.3420
0.	99.99	3956.0	24	-0.3420
0.	75.00	4000.0	24	-0.3420
0.	50.01	4043.0	23	-0.3420
0.	25.00	4083.0	23	-0.3420
0.	0.00	4122.0	23	-0.3420

*In BOSOR4, an eccentricity of 0.312 inches is input. BOSOR4 measures from the shell wall surface.

Effect of Boundary Conditions

The boundary conditions significantly affect the response of a stiffened shell.[5,6] A ring section or repeating element model of a ring- and stringer-stiffened shell is created with only one ring frame. In Fig. 12, a

picture of the model in its undeformed shape is presented. Two models are created to investigate the behavior of the shell in the interior, away from edge effects. One has internal stiffening and the other has external stiffening. The boundary conditions for the models has symmetry conditions at each end, Table 4. One end is allowed to move axially to introduce the axial load into the shell. The opposite end is not allowed to move in the axial direction.

When loaded under axial compression the externally stiffened shell carries a higher load ($Nx_{int.}$ 3816 lbs/in. vs. $Nx_{ext.}$ = 4972 lbs/in.), but for temperature load, it tolerates a similar amount of temperature change ($T_{int.}$ 486°F vs. $T_{ext.}$ = 499°F). The two buckling interaction curves are similar and actually come together as the temperature rises, Fig. 13. Clamping of the boundaries plays an important role on the behavior of the shells. The clamping causes the two models to have the same mode shape along the entire buckling interaction curve, Fig. 12.

A comparison of the results for the single-ring models with the full-length model suggests that the critical axial loads are less dependent on the boundary conditions. However, a comparison of the thermal buckling results indicates that boundary conditions are critical.

IV. Concluding Remarks

A numerical study of the buckling behavior of a generic stiffened shell has been presented. Analysis of buckling under combined mechanical load and thermal load was conducted using a finite difference shell-of-revolution code. The thermal buckling analysis corresponds to the case where the shell skin was heated, but the rings, stringers and ends of the shell remained cool. Longitudinally stiffened shells with and without ring frames were considered.

Results for the shell with only longitudinal stiffening indicated a large difference in buckling effects from the positioning of eccentric stiffening. Under thermal load alone, internally stiffened shells withstood a temperature change of almost three times that of externally stiffened shells. The trend reversed when there is only mechanical load. The internally stiffened shell carried roughly half the axial load of the externally stiffened shell.

The stiffener eccentricity effects were more moderate for the ring- and stringer-stiffened shell. Under only thermal loading, the internally stiffened shell withstood twice the temperature change of the comparable shell with external longitudinal stiffening. The shells with external longitudinal stringers withstood a greater mechanical load than shells with internal stringers and rings.

A comparison of results for single-ring (interior) stiffened shells with results for a six ring-stiffened shell indicated that for axial compressive load, the buckling results were similar. The eccentricity effects were quite different for thermal buckling, with virtually no effect on the one-ring shells. As noted by previous investigators (e.g., ref. 5), thermal buckling was strongly related to boundary conditions. The present paper showed that eccentricity effects in thermal buckling were also greatly affected by edge effects.

Finally, the eccentricity trends in the present paper need more investigation. The effects of pre-buckling deformations and loads, buckling boundary conditions, modeling techniques, and in-depth studies of the underlying equations and solutions used in analyzing thermal buckling of shells could all be subjects for future investigations. A physical experiment should be conducted to verify the trends discovered in this research.

V. Acknowledgment

The authors express their appreciation to David Bushnell for running some cases and helpful discussions on thermal buckling phenomena.

VI. References

1. Bushnell, D., "BOSOR4: Program for Stress and Vibration of Shells of Revolution," *Structural Mechanics Software Series - Vol. 1*, Edited by N. Perrone and W. Pilkey, University Press of Virginia, Charlottesville, VA, pp. 11-143, 1977.

2. Bushnell, D., "Stress, Stability and Vibration of Complex Shells of Revolution: Analysis and User's Manual for BOSOR4, "NASA CR-2115, Oct. 1972.

3. Corning, G., *Supersonic and Subsonic Airplane Design*, 3rd Edition, 7th Printing, Braun-Brumfield, Inc., Ann Arbor, Mich., 1970, p. 484.

4. Chang, L.K. and Card, M.F., "Thermal Buckling Analysis for Stiffened Orthotropic Cylindrical Shells," NASA TN-D-6332, 1971.

5. Ross, B., Hoff, N. J., and Horton, W. H., "The Buckling Behavior of Uniformly Heated Thin Circular Cylindrical Shells," *Experimental Mechanics*, Vol. 6 Nov., 1966, pp. 529-537; also in *Monocoque, Sandwich and Composite Aerospace Structures - Selected Papers of Nicholas J. Hoff,* Technomic Publishing Company, Lancaster, PA, 1986, pp. 313-321.

6. Anderson, M. S., "Thermal Buckling of Cylinders," Collected Papers on Instability of Shell Structures, NASA TN-D-1510, 1962, pp. 267-276.

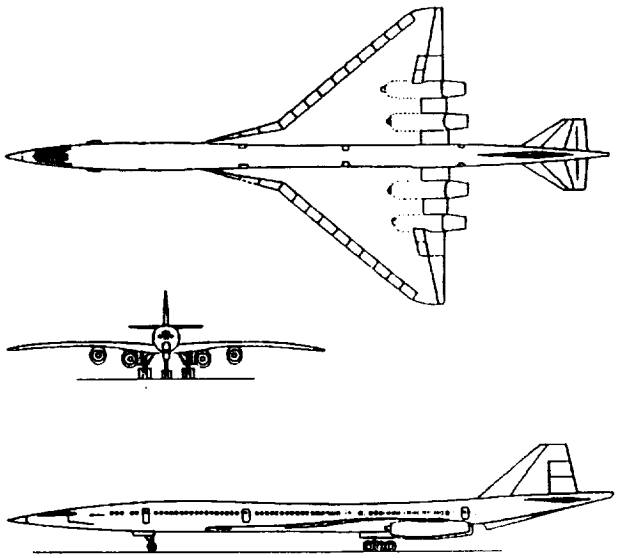

Fig. 1 Sketch of the early (1970) U.S. Supersonic Transport (SST).

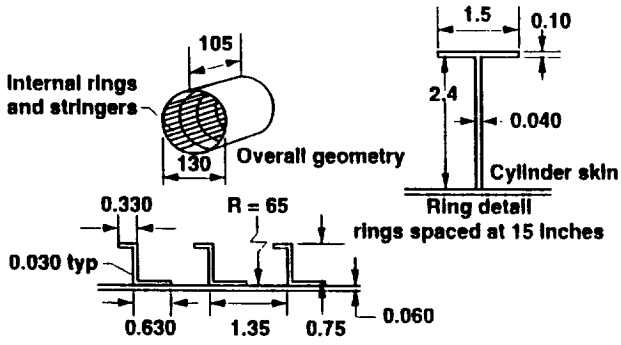

Fig. 2 Geometry of a typical ring- and stringer-stiffened shell analyzed in BOSOR4. Dimensions are in inches.

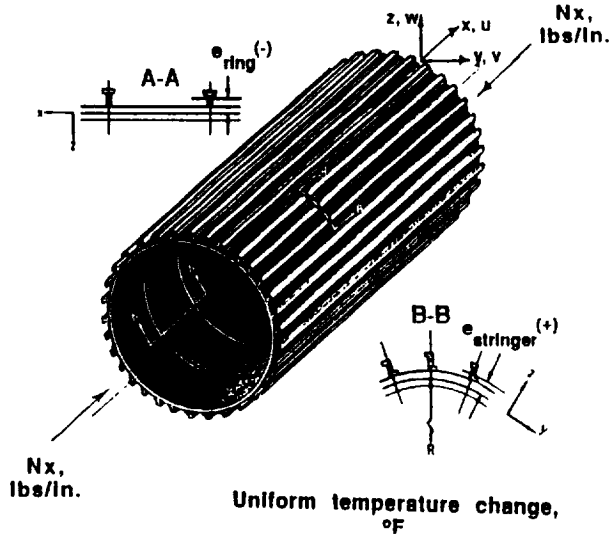

Fig. 3 Coordinate system of the shell model, placement of loads and depiction of stiffener eccentricities.

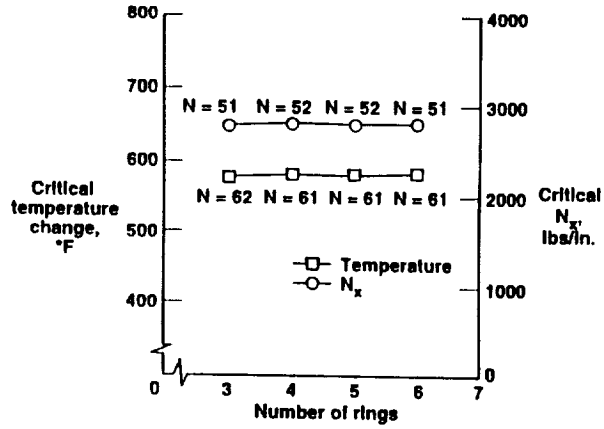

Fig. 4 Effect of number of rings on the critical buckling temperature and critical axial load.

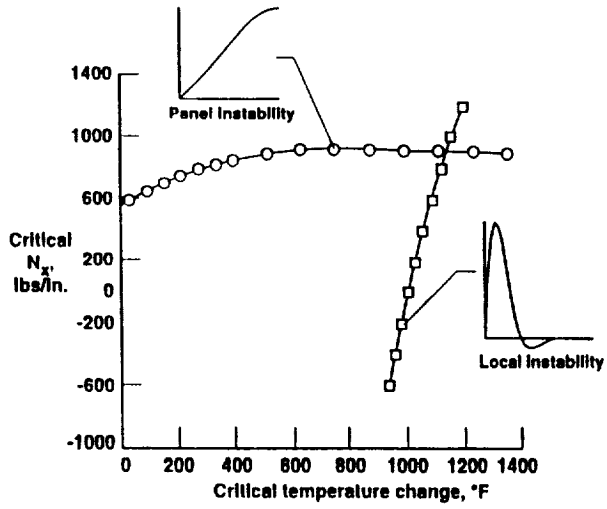

Fig. 5 Buckling interaction curve and associated mode shapes for a shell with stringers at an eccentricity of -0.342 inches (internal).

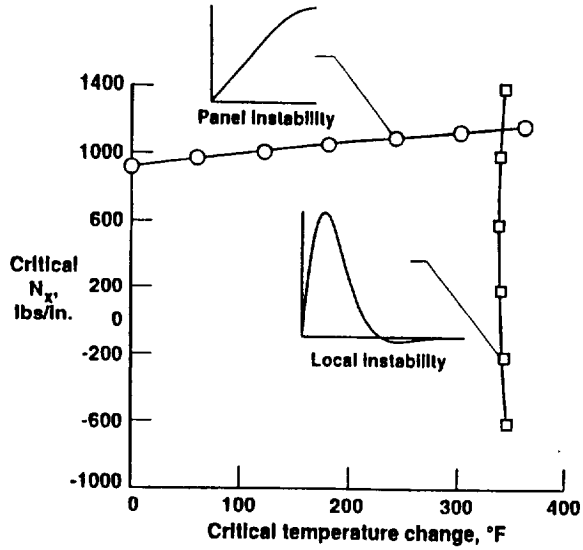

Fig. 6 Buckling interaction curve and associated mode shapes for a shell with stringers at an eccentricity of 0.342 inches (external).

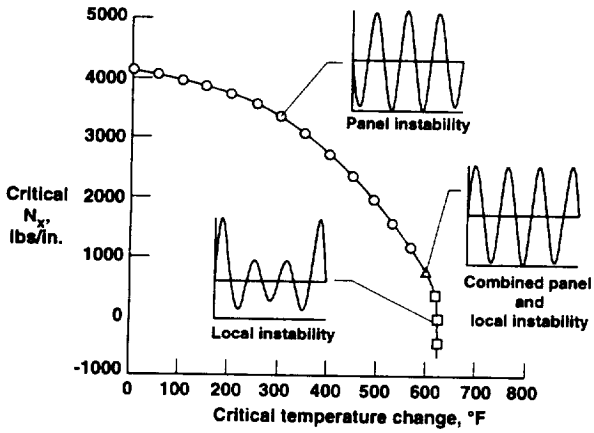

Fig. 7 Buckling interaction curve and associated mode shapes for a shell with internal ring frames and stringers at an eccentricity of -0.342 inches (internal).

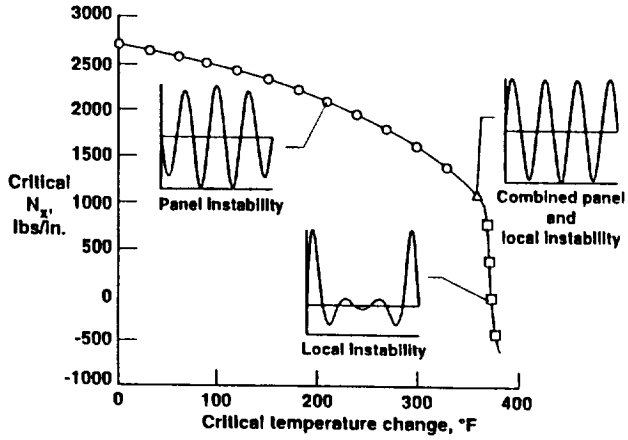

Fig. 8 Buckling interaction curve and associated mode shapes for a shell with internal ring frames and stringers at an eccentricity of 0.000 inches.

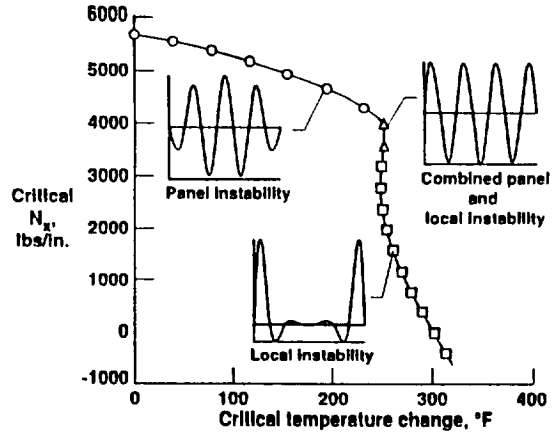

Fig. 9 Buckling interaction curve and associated mode shapes for a shell with internal ring frames and stringers at an eccentricity of 0.342 inches (external).

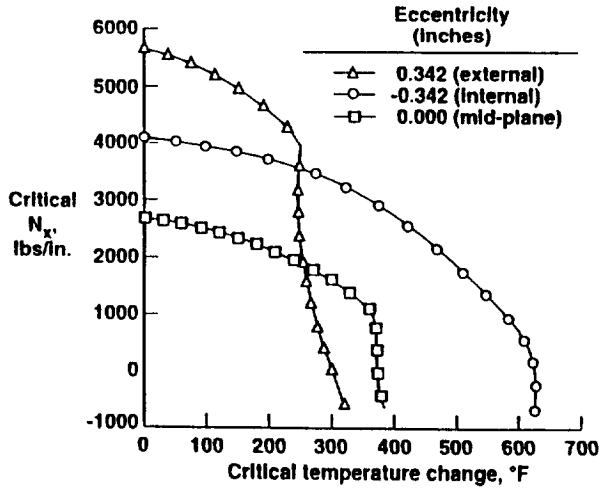

Fig. 10 Comparison of buckling interaction curves for three eccentricities.

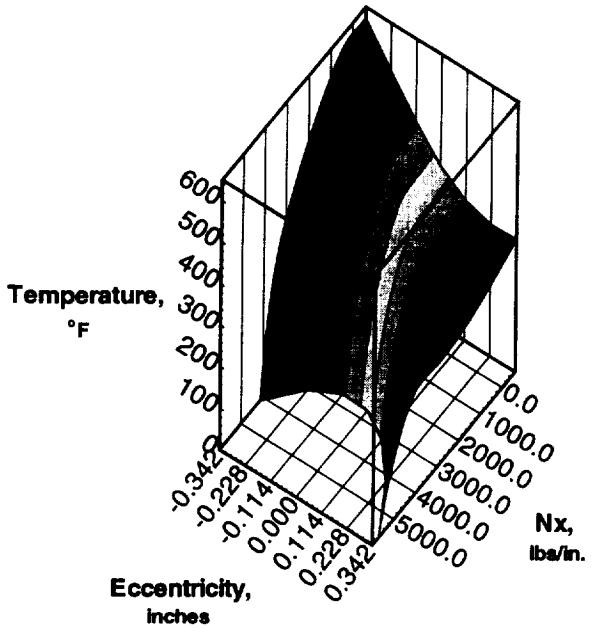

Fig. 11 Buckling interaction surface for a ring- and stringer-stiffened shell.

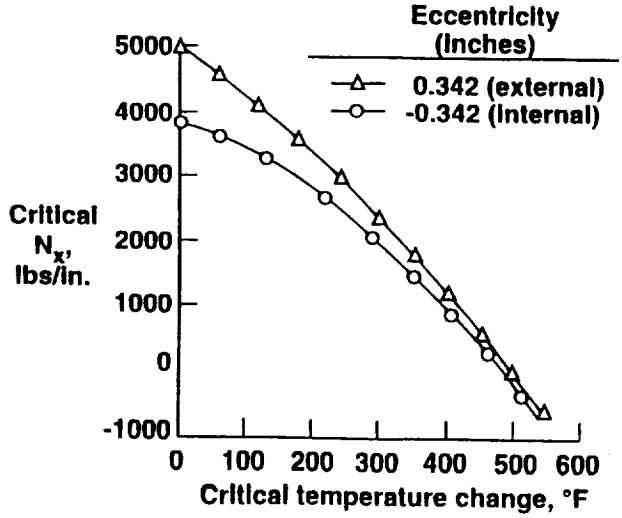

Fig. 13 Buckling interaction curves a stiffened single-ring model (repeating element model) with either internal- or external-longitudinal stiffening at an eccentricity of 0.342 inches.

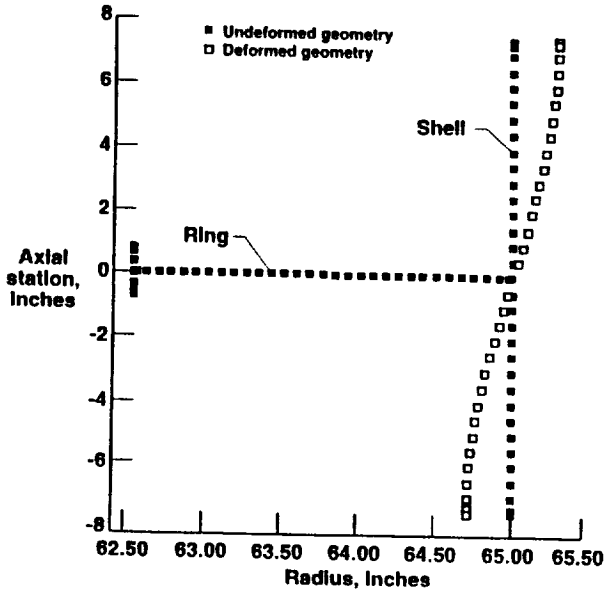

Fig. 12 Mode shape (panel instability) for a stiffened single-ring model (repeating element model) with either internal- or external-longitudinal stiffening at an eccentricity of 0.342 inches.